

Supplementary information

Ultrafast coherent photoexcited dynamics in a trimeric dendrimer probed by X-ray stimulated-Raman signals

Victor M. Freixas^{†1}, Daniel Keefer^{†2}, Sergei Tretiak³, Sebastian Fernandez-Alberti¹,
Shaul Mukamel^{*2}

¹*Departamento de Ciencia y Tecnología, Universidad Nacional de Quilmes/CONICET,
B1876B XD, Bernal, Argentina*

²*Department of Chemistry and Physics and Astronomy, University of California, Irvine,
California 92697-2025, USA*

³*Theoretical Division, Los Alamos National Laboratory, Los Alamos, New Mexico 87545,
United States*

[†] These authors contributed equally

*smukamel@uci.edu

Contents

A Cloning criteria and thresholds	S2
B Fraction of transition density	S5
C Parameters of the fit to eq. (1)	S6
D Pure electronic dephasing	S7
E Surface hopping simulations	S8
F Transition density matrix snapshots	S9
G Non-adiabatic coupling analysis	S11
H Additional Trajectories	S13
I Frenkel exciton model	S17

A Cloning criteria and thresholds

- *Criteria #1:*

Cloning should take place in situations where more than one excited state is significantly populated. This can be monitored by the distribution width W_n [1]:

$$W_n = \frac{1}{\sum_I^N |a_I^{(n)}|^4} \quad . \quad (\text{S1})$$

W_n takes values between 1 and the total number of excited states considered N . Values near 1 means that all the population is concentrated in a single state, while values near N means an even distribution. Therefore, the cloning events were restricted to situations where:

$$W_n > \delta_1 = 2.0 \quad . \quad (\text{S2})$$

The time evolution of the expectation value of W_n might be misleading in the sense that it has a broad distribution and presents sudden changes after cloning events. Moreover, it only quantifies whether the electronic populations for a given trajectory spread over the different states or not. A more decisive criterion is the breaking angle defined in criteria #2: the populations might be distributed over several states, but if all those states pull the nuclear system in the same direction of motion there is no need for bifurcating the wavefunction. Figure S1 depicts the distribution of values of W_n for all time steps and trajectories of the complete ensemble for the current case. The peak at approximately $W_n = 2$ is associated to the threshold $\delta_1 = 2$, while the peak at approximately $W_n = 1$ is associated either to the subsequent reduction of W_n after each cloning event or to values acquired after electronic energy relaxation to the S_1 state.

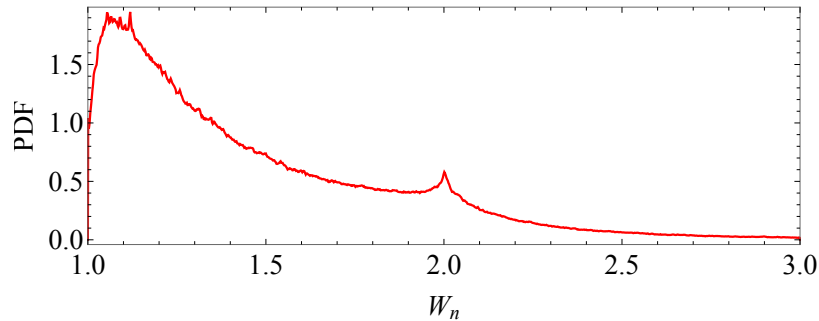


Figure S1: Probability density function (PDF) of W_n defined according to (eq. S1) for all trajectories and time steps of the complete ensemble for the current case.

- *Criteria #2:*

Cloning should take place in situations where the wavepacket would split in configuration space. This is monitored by the breaking angle [1]:

$$\theta^{(n)} = \arccos \left(\frac{2\mathbf{F}_M^{(n)} \cdot \mathbf{F}_{max}^{(n)}}{|\mathbf{F}_M^{(n)}|^2 + |\mathbf{F}_{max}^{(n)}|^2} \right) \quad , \quad (\text{S3})$$

where $\mathbf{F}_M^{(n)}$ is the averaged excited state gradient for configuration n :

$$\mathbf{F}_M^{(n)} = - \sum_I \left| a_I^{(n)} \right|^2 \nabla_{\mathbf{R}_n} V_I^{(n)} \quad , \quad (\text{S4})$$

where \mathbf{R}_n represents the nuclear coordinates for configuration n and $V_I^{(n)}$ represents the energy corresponding to the excited state I of configuration n . $\mathbf{F}_{max}^{(n)}$ is minus the gradient corresponding to the most populated state. By restricting the cloning events to situations in which:

$$\theta^{(n)} > \delta_2 = 10^\circ \quad , \quad (\text{S5})$$

we ensure that the two new configurations produced after a cloning event will split in configuration space providing the desired bifurcation effect and rectifying the physical meaning of the mean field.

- *Criteria #3:*

In order to make the algorithm efficient and avoid a overproduction of cloning events in the strong coupling regions of configuration space, we avoid cloning when the coupling is to high. By this way clones are produced once the system leaves strong coupling regions if the two previous criteria are fulfilled. The coupling is monitored in similar fashion as the quantum transition probability is calculated for the fewest switches surface hopping algorithm [2, 3]:

$$\sum_I \left| \frac{2\sigma_I^{(n)} \cos\left(\theta_I^{(n)} - \theta_{max}^{(n)}\right) \dot{\mathbf{R}}_n \cdot \mathbf{d}_{I,max}^{(n)}}{\sigma_{max}} \right| < \delta_3 \quad , \quad (\text{S6})$$

where $\sigma_I^{(n)}$ and $\theta_I^{(n)}$ are the modulus and phase corresponding to the electronic amplitudes $a_I^{(n)}$, the index max refers to the most populated state, $\dot{\mathbf{R}}_n$ is the nuclear velocity in configuration n and $\mathbf{d}_{I,max}^{(n)}$ is the non-adiabatic coupling between excited states I and the one with the greater population for configuration n :

$$\mathbf{d}_{I,max}^{(n)} = \langle \phi_I^{(n)} | \nabla_{\mathbf{R}_n} | \phi_{max}^{(n)} \rangle \quad . \quad (\text{S7})$$

Therefore, by setting $\delta_3 = 0.05$ we ensure an efficient clone generation away from the strong coupling regions of configuration space.

- *Criteria #4:*

The nuclear amplitude corresponding to each configuration splits after a cloning event. If the total number of clones is not controlled, an exponential growth, with an exponentially decreasing weight for the corresponding configurations, would make the algorithm too inefficient. Therefore, we allowed a total of 4 consecutive clones, leading to a maximum of 16 clones per initial condition. Previous convergence tests have shown that there is no a relevant accuracy improvement after the production of approximately 14 clones per initial condition [2]. In the current case, an average of approximately 6 clones per initial condition were generated. These clones take place through out all the simulation time. Figure S2 shows that cloning events occurs during the simulations in an homogeneous rate.

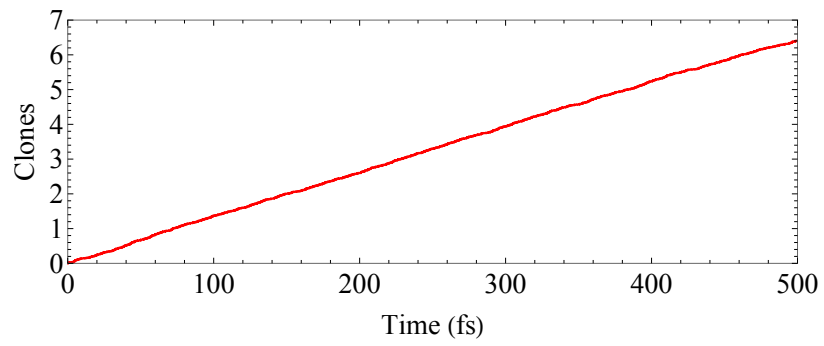


Figure S2: Average number of cloning events per initial condition as a function of time.

B Fraction of transition density

Within the Collective Electronic Oscillator (CEO) approach the Configuration Interaction Singlet (CIS) eigenstate I for configuration n , written in Atomic Orbitals (AO) basis, is denoted frequently as transition density matrices [4, 5, 6]:

$$\left(\rho_I^{(n)}\right)_{i,j} = \langle \phi_I^{(n)} | \hat{c}_i^\dagger \hat{c}_j | \phi_g^{(n)} \rangle \quad , \quad (\text{S8})$$

where $|\phi_g^{(n)}\rangle$ is the ground state wavefunction, and \hat{c}_i^\dagger and \hat{c}_j are the electron creation and annihilation operators with indexes i and j referring to AO basis functions. Diagonal elements $\left(\rho_I^{(n)}\right)_{i,i}$ are relevant to the changes in the distribution of electronic density in the i th orbital in the case of bound excitonic states caused by excitation [7].

During AIMC simulations, the intramolecular electronic energy redistribution can be followed using the time-dependent spatial localization of $\rho_I^{(n)}$. The fraction of transition density localized on a specific segment X of the molecule can be defined as [1]:

$$\rho_{I,X}^{(n)} = \frac{\sum_{i \in X} \left(\rho_I^{(n)}\right)_{i,i}^2}{\sum_i \left(\rho_I^{(n)}\right)_{i,i}^2} \quad . \quad (\text{S9})$$

In order to calculate the corresponding expectation value for the Multiconfigurational Ehrenfest (MCE) wavefunction we can introduce the operator $\hat{\rho}_X$ such that:

$$\hat{\rho}_X |\phi_I^{(n)}\rangle = \rho_{I,X}^{(n)} |\phi_I^{(n)}\rangle \quad , \quad (\text{S10})$$

which expectation value can be calculated as:

$$\langle \hat{\rho}_X \rangle = \Re \left\{ \sum_{n,m} c_m^* c_n \langle \chi_m | \chi_n \rangle \sum_{I,J} \left(a_I^{(m)}\right)^* a_J^{(n)} \langle \phi_I^{(m)} | \phi_J^{(n)} \rangle \rho_{I,X}^{(m)} \right\} \quad , \quad (\text{S11})$$

where \Re stands for the real part.

C Parameters of the fit to eq. (1)

The function in eq. (1) describes the relaxation process to S_1 as a superposition of an exponential decay plus an exponentially damped oscillation, such that both contributions have the same weight at $t = 0$. Parameters a and b corresponds to the asymptotic value of S_1 population and its initial value, respectively; τ_1 is the S_1 decay time, T is the period of the vibronic oscillations and τ_2 is the vibronic decoherence time. R is the corresponding R -squared.

Parameter	Estimate	Standard error
a	0.81	0.00
b	0.24	0.00
$\tau_1(fs)$	5.42	0.04
$T(fs)$	19.96	0.02
$\tau_2(fs)$	23.31	0.12
R	0.9999	—

Table S1: Parameters obtained by fitting the population of S_1 in Figure 2(a) to $f(t)$ given by eq. (1).

D Pure electronic dephasing

Within linear response theory [8], the correlation between excited states I and J is quantified by the autocorrelation function:

$$C_{IJ} = \langle \delta E_{IJ}(t) \delta E_{IJ}(0) \rangle, \quad (\text{S12})$$

where δE_{IJ} is the corresponding energy gap and the angular brackets means average over the ensemble. The energy corresponding to a given state K is calculated as the expectation value:

$$\begin{aligned} E_K &= \langle \Psi | \hat{E}_K | \Psi \rangle = \\ &= \sum_{n,m} (c_m)^* c_n \langle \chi_m | \chi_n \rangle E_K^{(n)} \sum_{IJ} \left(a_I^{(m)} \right)^* a_J^{(n)} \langle \phi_I^{(m)} | \phi_J^{(n)} \rangle, \end{aligned} \quad (\text{S13})$$

where $E_K^{(n)}$ is the energy corresponding to the adiabatic state K for the center of configuration n .

The pure electronic dephasing $D_{IJ}(t)$ is defined by the second order cumulant approximation [8]:

$$D_{IJ} = \exp \left(-\frac{1}{\hbar^2} \int_0^t dt' \int_0^{t'} dt'' C_{IJ}(t) \right). \quad (\text{S14})$$

Finally, the pure electronic decoherence time τ_{IJ} can be obtained by fitting the pure dephasing D_{IJ} to a Gaussian function:

$$D_{IJ} \approx \exp \left(-\left(\frac{t}{\tau_{IJ}} \right)^2 \right). \quad (\text{S15})$$

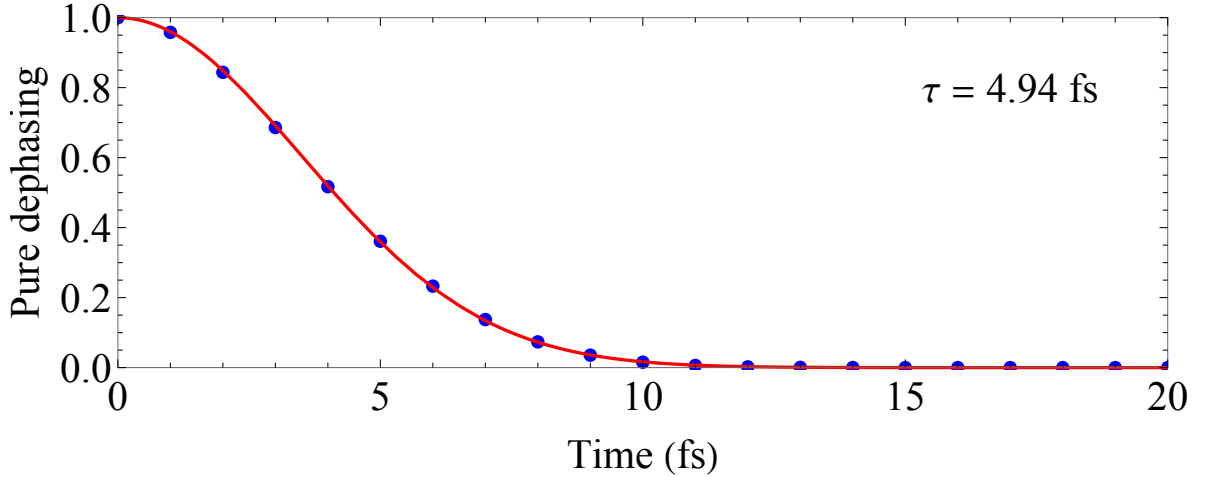


Figure S3: Pure electronic dephasing function for the triarylamine trimer $D_{12}(t)$ evaluated from the AIMC simulations.

E Surface hopping simulations

NEXMD surface hopping (SH) simulations were performed in order to compare the capability of the SH method to reproduce the oscillatory behavior of the electronic populations resulting from vibronic coherences. The same ensemble of initial configurations as for AIMC simulations has been considered. The electronic wavefunction was collapsed to S_2 at $t = 0$ in order to maximize the appearance of any possible oscillations. Figure (S4) shows the electronic populations, calculated as the fraction of trajectories evolving on each state at any given time. NEXMD-SH simulations were performed at a constant energy. Classical time steps of 0.1 fs have been used for the propagation of nuclei in ground state and a quantum time step of 0.025 fs has been used to propagate the electronic degrees of freedom. Corrections for decoherence [9], parameters and the methodology of NEXMD-SH simulations have been extensively discussed elsewhere [10].

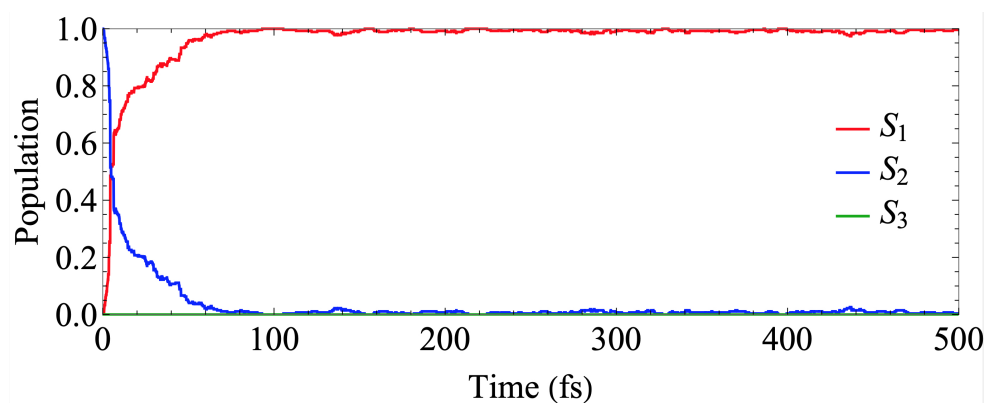


Figure S4: Time evolution of the electronic populations for SH dynamics.

F Transition density matrix snapshots

In order to calculate transition density matrix for the MCE wavefunction $|\Psi\rangle$, we first calculate the expectation value of the transition density matrix from the ground state to a given state K :

$$\begin{aligned}\rho_K &= \langle \Psi | \hat{\rho}_{0K} | \Psi \rangle = \\ &= \sum_{n,m} (c_m)^* c_n \langle \chi_m | \chi_n \rangle \rho_{0K}^{(n)} \sum_{IJ} \left(a_I^{(m)} \right)^* a_J^{(n)} \langle \phi_I^{(m)} | \phi_J^{(n)} \rangle,\end{aligned}\quad (\text{S16})$$

where $\rho_{0K}^{(n)}$ is the transition density matrix [7] from the ground state to excited state K for the center of configuration n .

The transition density matrix ρ from the ground state to the superposition of excited states is then calculated as:

$$\rho = \sum_K |a_K|^2 \rho_K, \quad (\text{S17})$$

where a_K is calculated according to [1]:

$$|a_K|^2 = \Re \left\{ \sum_{n,m} (c_m)^* c_n \langle \chi_m | \chi_n \rangle \left(a_K^{(m)} \right)^* \sum_I a_I^{(n)} \langle \phi_K^{(m)} | \phi_I^{(n)} \rangle \right\}. \quad (\text{S18})$$

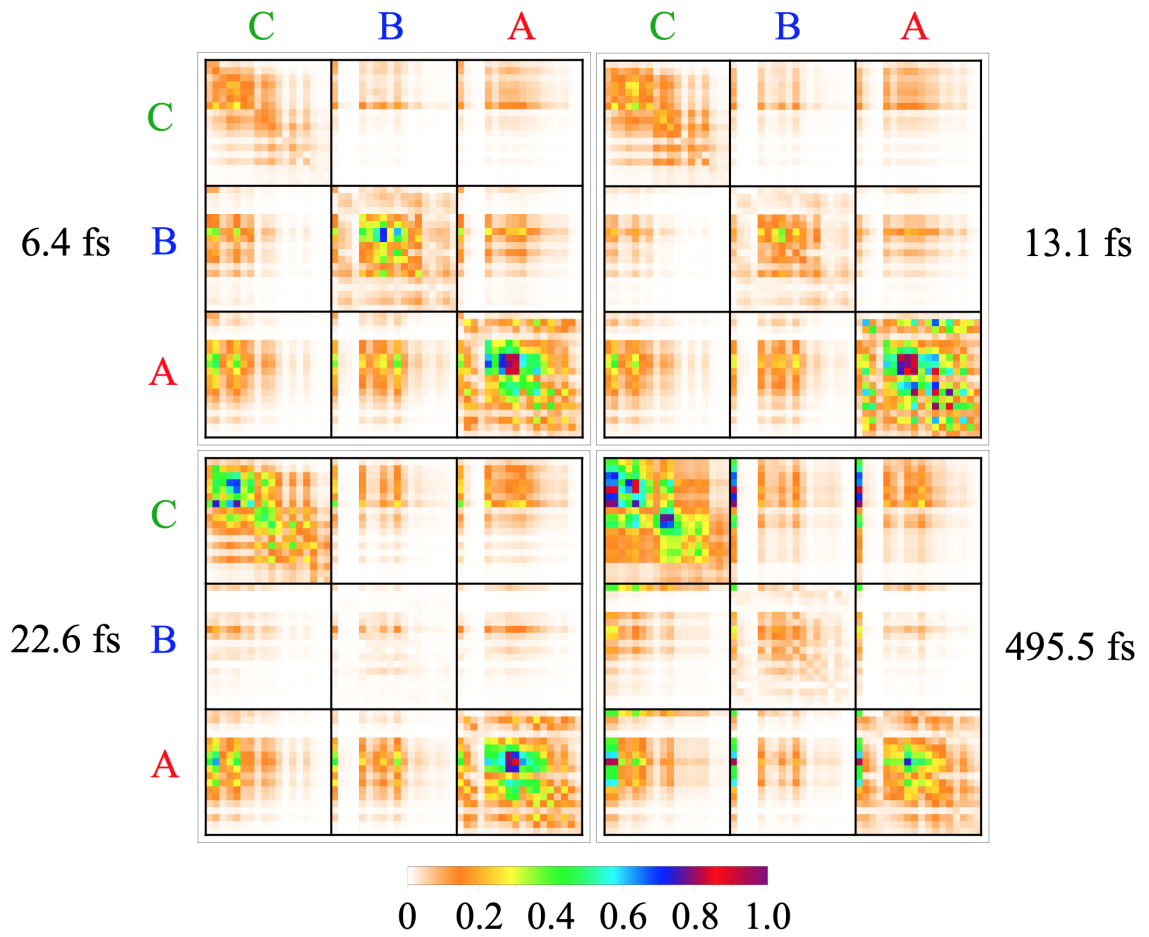


Figure S5: Transition density matrices (eq. (S17)) corresponding to the the different snapshots shown in Figure 3(a).

G Non-adiabatic coupling analysis

A further insight into the vibronic dynamics can be achieved by analyzing the nonadiabatic coupling vector (NACR) in regions of strong coupling near conical intersection seams. The strong coupling regime is defined as situations where the absolute value of NACR is higher than its mean value plus 10 times the standard deviation during each AIMC trajectory. Figure S6(a) shows a real-space representation of a typical NACR. We find that NACR involves antisymmetric nuclear motions on two of the three branches. This behavior involving antisymmetric motions on different branches of a dendrimer has been reported previously [11] and was associated to the fact that the molecular wavefunction adopts a standing wave pattern according to the particle (exciton) in a box model and the $S_2 \rightarrow S_1$ transition can be associated with a transition where symmetry between states changes. That is, the vibronic excitation has an antisymmetric form where the two branches experience structural deformations with opposite phases (i.e. expansion and compression). Figure S6(b) depicts the probability density function of the fraction of NACR absolute values localized on the three branches, denoted as I, II, and III according to their corresponding contribution values in a decreasing order. We can observe that the NACRs are not equally distributed among the three branches but localized mainly in two of them. The distribution of the projections of NACR onto the normal modes basis, calculated at the S_1 minimum energy configuration, is shown in Figure S6(c). The peak at ~ 19 fs (~ 1750 cm^{-1}) matches the period T of the vibronic oscillations (~ 20 fs) obtained by fitting the evolution in time of the S_1 population (see Figure 2(a) and Table S1). Vibronic dynamics are thus assisted by a reduced set of high-frequency normal modes.

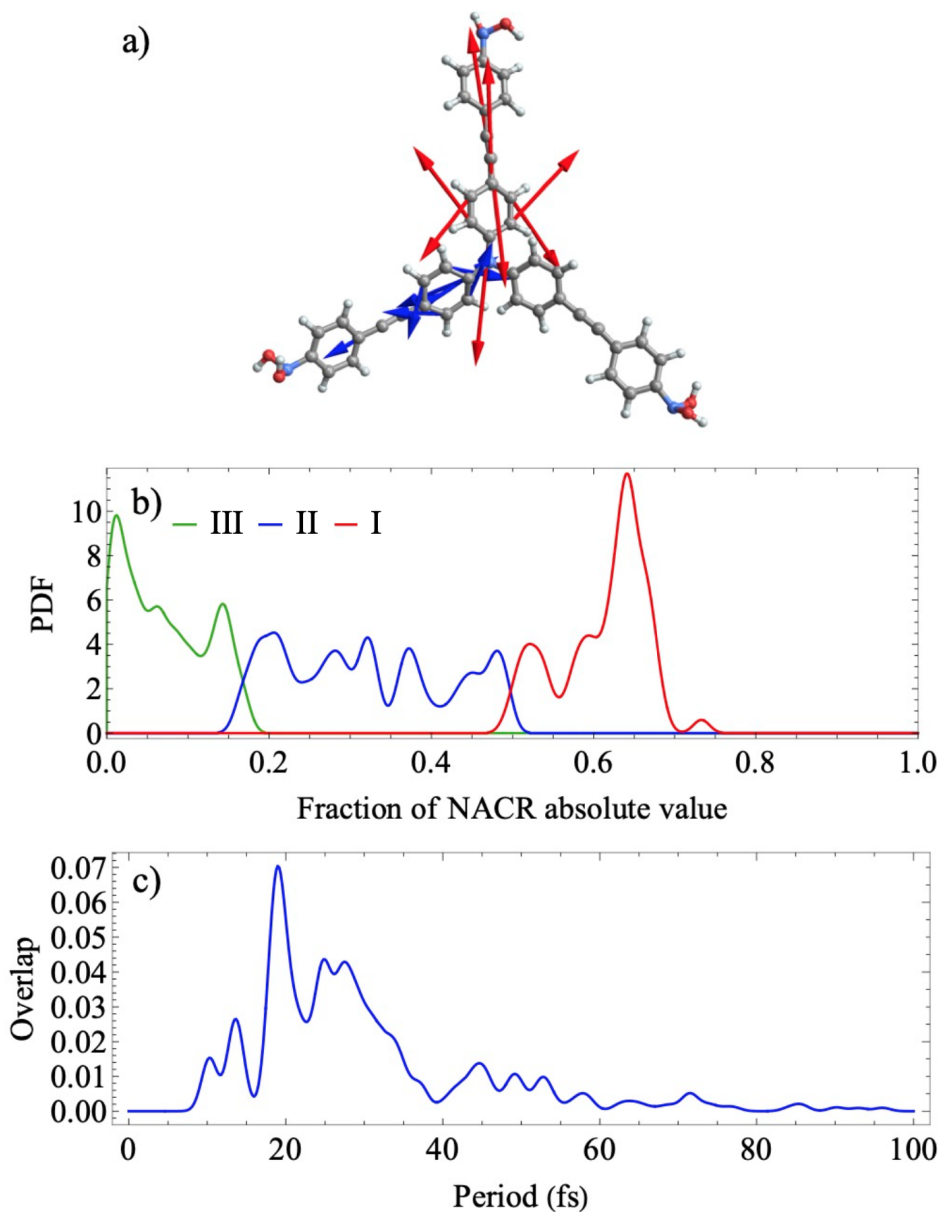


Figure S6: (a) Representation of a typical NACR in real space during a region of strong coupling between states. (b) Probability density function of the fraction of NACR absolute values during strong coupling regime. For each AIMC trajectory, branches I, II, and III are sorted according to their corresponding fractions of NACR absolute value in decreasing order. (c) Distribution of the overlap between nuclear normal modes, calculated at the S_1 minimum energy configuration, and the NACR at configurations of strong coupling.

H Additional Trajectories

Only trajectory 2 is discussed in the main text. This trajectory is representative of a large fraction of trajectories in the ensemble, with only minor differences especially in the signal. Here, we discuss a few interesting trajectories to give a better impression about the range of properties during the dynamics.

- Figure S7 shows a trajectory that is similar to trajectory 2 in the main text, but where the transition density is located in branches A and C instead of B and C. This exemplifies that most trajectories are quite similar and the three branches of the molecule are equal, while the transition density is localized in two of them simultaneously.
- Figure S8 depicts a trajectory where the ρ_{13} contribution to the signal is equally strong to the usually dominating ρ_{12} contribution. Thus, they are both well visible in the total signal of this trajectory and well distinguishable at different Raman shifts.
- In Figure S9, trajectory 5 exhibits much larger and more frequent population oscillations, especially between S_1 and S_2 . This does not considerably affect the relative magnitudes and persistence of the individual signal contributions, however.

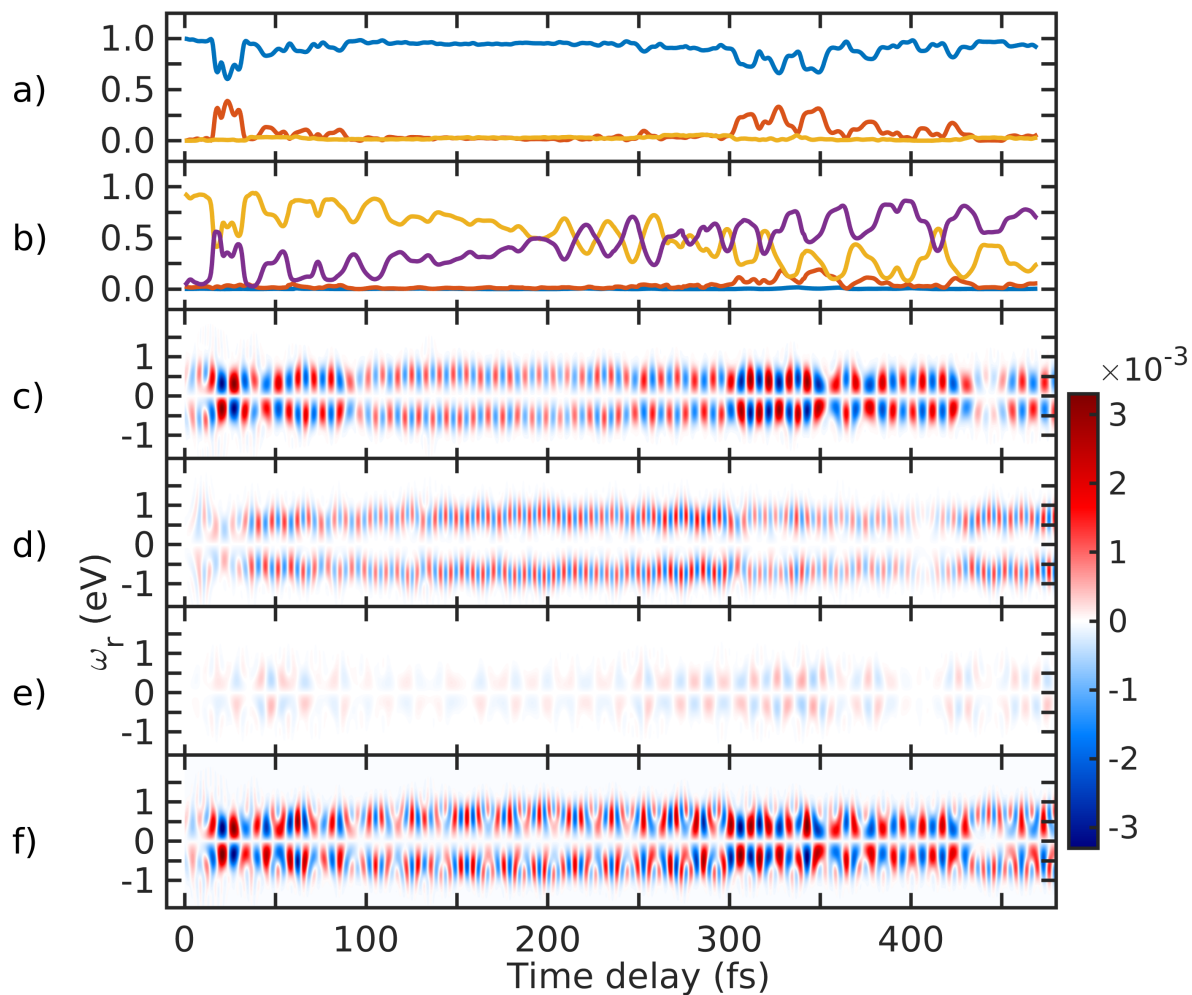


Figure S7: Dynamics and TRUECARs signal in trajectory 3. **a)** Populations in the S_1 (blue), S_2 (red) and S_3 (yellow) states. **b)** Fraction of transition density in branch A (purple), B (yellow), C (red) and around the central Nitrogen (blue). **c)** Frequency-dispersed TRUECARs signal (eq. 2) for the coherence ρ_{12} between S_1 and S_2 . **d–e)** same as c) for ρ_{13} and ρ_{23} . **f)** Total TRUECARs signal for trajectory 2 given by the sum of c–e.

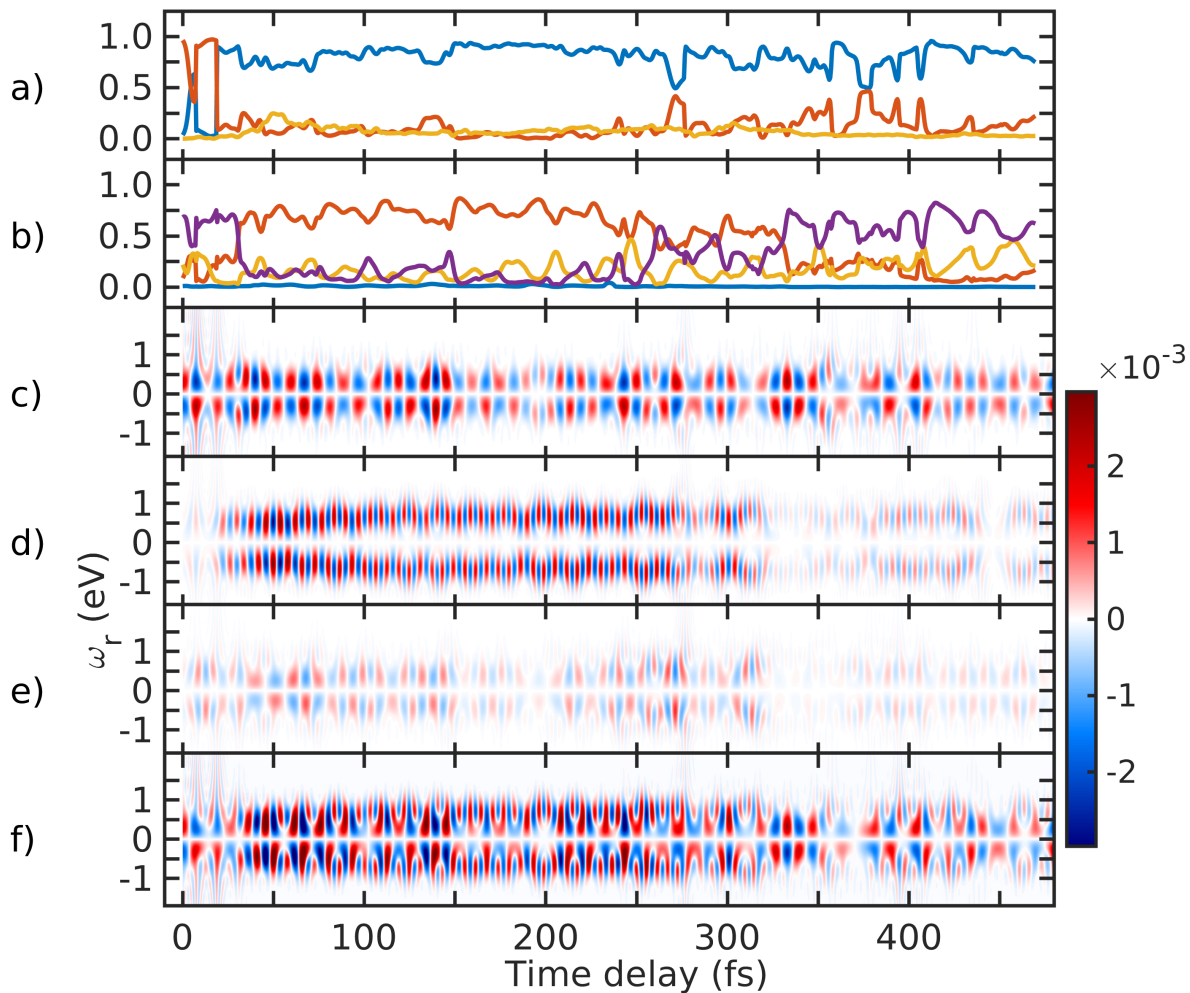


Figure S8: Dynamics and TRUECARs signal in trajectory 4. **a)** Populations in the S_1 (blue), S_2 (red) and S_3 (yellow) states. **b)** Fraction of transition density in branch A (purple), B (yellow), C (red) and around the central Nitrogen (blue). **c)** Frequency-dispersed TRUECARs signal (eq. 2) for the coherence ρ_{12} between S_1 and S_2 . **d–e)** same as c) for ρ_{13} and ρ_{23} . **f)** Total TRUECARs signal for trajectory 2 given by the sum of c–e.

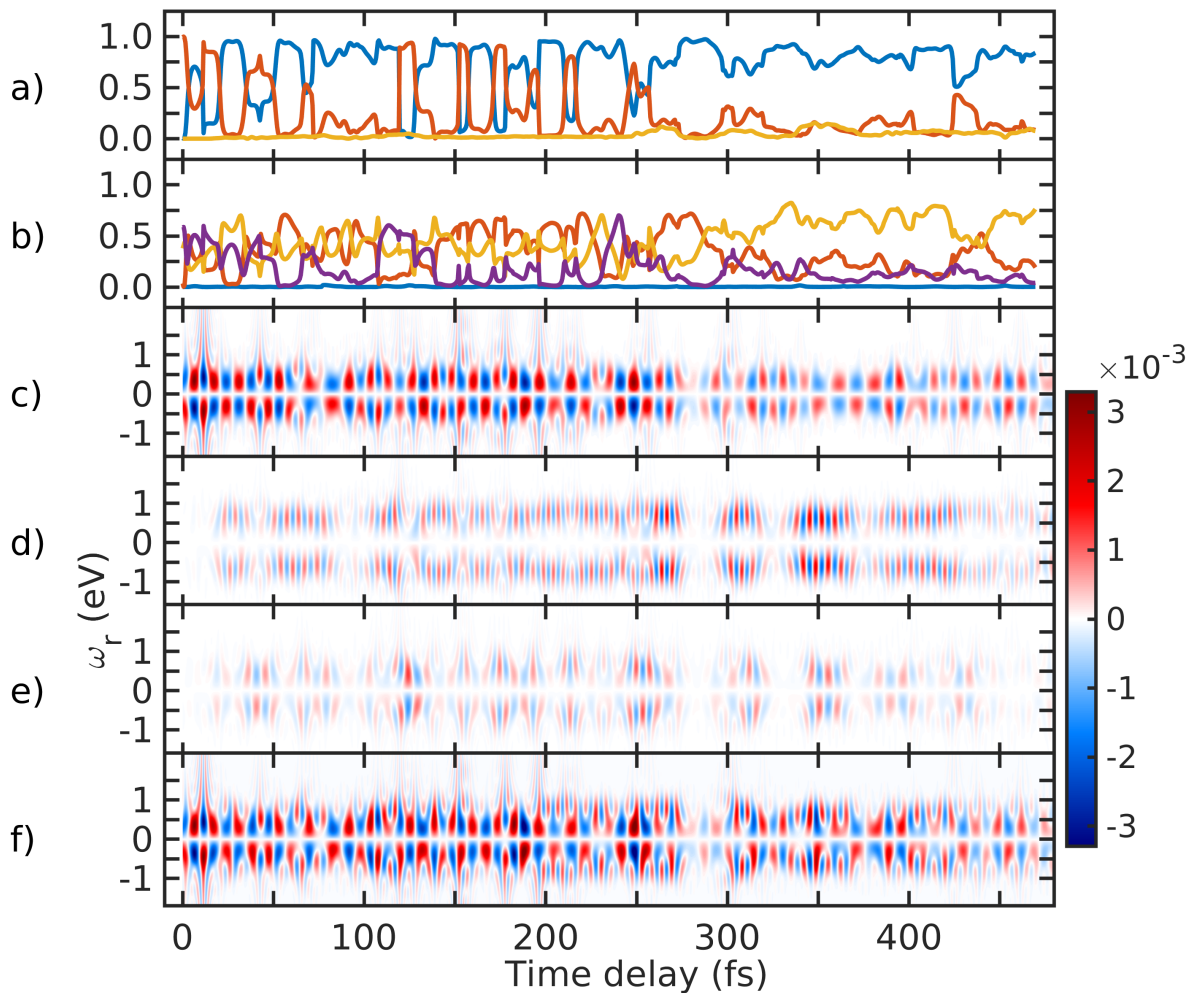


Figure S9: Dynamics and TRUECARs signal in trajectory 5. **a)** Populations in the S_1 (blue), S_2 (red) and S_3 (yellow) states. **b)** Fraction of transition density in branch A (purple), B (yellow), C (red) and around the central Nitrogen (blue). **c)** Frequency-dispersed TRUECARs signal (eq. 2) for the coherence ρ_{12} between S_1 and S_2 . **d–e)** same as c) for ρ_{13} and ρ_{23} . **f)** Total TRUECARs signal for trajectory 2 given by the sum of c–e.

I Frenkel exciton model

In the Frenkel exciton model, the excited states of the trimer are considered as a linear combination of the solutions for the individual branches. In the perfect symmetry regime, and using the first solution E on each identical branch and a unique common coupling V between them as a basis, the Frenkel exciton Hamiltonian can be expressed as:

$$H = \begin{pmatrix} E & V & V \\ V & E & V \\ V & V & E \end{pmatrix}, \quad (\text{S19})$$

with eigenvalues:

$$\begin{aligned} E - V \\ E - V \\ E + 2V \end{aligned} \quad (\text{S20})$$

and eigenvectors:

$$\begin{pmatrix} -1 & 0 & 1 \\ -1 & 1 & 0 \\ 1 & 1 & 1 \end{pmatrix} \quad (\text{S21})$$

If we associate the S_1 and S_2 to the degenerate states with energies $E - V$, and S_3 with energy $E + 2V$, the coupling V can be estimated as one third of the energy splitting between S_1/S_2 and S_3 .

References

- [1] Victor M. Freixas, Sebastian Fernandez-Alberti, Dmitry V. Makhov, Sergei Tretiak, and Dmitrii Shalashilin. An ab initio multiple cloning approach for the simulation of photoinduced dynamics in conjugated molecules. *Phys. Chem. Chem. Phys.*, 20:17762–17772, 2018.
- [2] Victor M. Freixas, Alexander J. White, Tammie Nelson, Huajing Song, Dmitry V. Makhov, Dmitrii Shalashilin, Sebastian Fernandez-Alberti, and Sergei Tretiak. Nonadiabatic excited-state molecular dynamics methodologies: Comparison and convergence. *The Journal of Physical Chemistry Letters*, 12(11):2970–2982, 2021. PMID: 33730495.
- [3] Daniel Keefer, Victor M. Freixas, Huajing Song, Sergei Tretiak, Sebastian Fernandez-Alberti, and Shaul Mukamel. Monitoring molecular vibronic coherences in a bichromophoric molecule by ultrafast x-ray spectroscopy. *Chem. Sci.*, 12:5286–5294, 2021.
- [4] Shaul Mukamel, Sergei Tretiak, Thomas Wagersreiter, and Vladimir Chernyak. Electronic coherence and collective optical excitations of conjugated molecules. *Science*, 277(5327):781–787, 1997.
- [5] Sergei Tretiak, Vladimir Chernyak, and Shaul Mukamel. Recursive density-matrix-spectral-moment algorithm for molecular nonlinear polarizabilities. *The Journal of chemical physics*, 105(19):8914–8928, 1996.
- [6] Sergei Tretiak, Wei Min Zhang, Vladimir Chernyak, and Shaul Mukamel. Excitonic couplings and electronic coherence in bridged naphthalene dimers. *Proceedings of the National Academy of Sciences*, 96(23):13003–13008, 1999.
- [7] Sergei Tretiak and Shaul Mukamel. Density matrix analysis and simulation of electronic excitations in conjugated and aggregated molecules. *Chemical reviews*, 102(9):3171–3212, 2002.
- [8] Shaul Mukamel. *Principles of nonlinear optical spectroscopy*, volume 29. Oxford university press New York, 1995.
- [9] Tammie Nelson, Sebastian Fernandez-Alberti, Adrian E. Roitberg, and Sergei Tretiak. Nonadiabatic excited-state molecular dynamics: Treatment of electronic decoherence. *Journal of Chemical Physics*, 138:224111, 2013.
- [10] Tammie R. Nelson, Alexander White, Josiah A. J.; Bjorgaard, Andrew E. Sifain, Yu Zhang, Benjamin Nebgen, Sebastian Fernandez-Alberti, Dimitry Mozyrsky, Adrian E. Roitberg, and Sergei Tretiak. Non-adiabatic excited-state molecular dynamics: Theory and applications for modeling photophysics in extended molecular materials. *Chemical Review*, 120:2215–2287, 2020.
- [11] Tammie R. Nelson, Dianelys Ondarse-Alvarez, Nicolas Oldani, Beatriz Rodriguez-Hernandez, Laura Alfonso-Hernandez, Johan F. Galindo, Valeria D. Kleiman, Sebastian Fernandez-Alberti, Adrian E. Roitberg, and Sergei Tretiak. Coherent exciton-vibrational dynamics and energy transfer in conjugated organics. *Nature Communications*, 9:2316, 2018.